

Tilt-Ropter: A Novel Hybrid Aerial and Terrestrial Vehicle with Tilt Rotors and Passive Wheels

Ruoyu Wang^{1,2}, Xuchen Liu^{1,3}, Zongzhou Wu¹, Zixuan Guo¹, Wendi Ding¹, Ben M. Chen¹

Abstract—In this work, we present Tilt-Ropter, a novel hybrid aerial-terrestrial vehicle (HATV) that combines tilt rotors with passive wheels to achieve energy-efficient multi-mode locomotion. Unlike existing under-actuated HATVs, the fully actuated design of Tilt-Ropter enables decoupled force and torque control, greatly enhancing its mobility and environmental adaptability.

A nonlinear model predictive controller (NMPC) is developed to track reference trajectories and handle contact constraints across locomotion modes, while a dedicated control allocation module exploits actuation redundancy to achieve energy-efficient control of actuators. Additionally, to enhance robustness during ground contact, we introduce an external wrench estimation algorithm that estimates environmental interaction forces and torques in real time.

The system is validated through both simulation and real-world experiments, including seamless air-ground transitions and trajectory tracking. Results show low tracking errors in both modes and highlight a 92.8% reduction in power consumption during ground locomotion, demonstrating the system’s potential for long-duration missions across large-scale and energy-constrained environments.

I. INTRODUCTION

In recent years, micro air vehicles (MAVs) have been widely applied in diverse real-world scenarios to improve working efficiency and reduce the risk of human operators. However, endurance remains a significant limitation, especially for applications that demand persistent operation, such as large-scale infrastructure inspection or long-duration surveillance. In such missions, MAVs often consume substantial energy when traveling between waypoints, and their limited battery capacity prevents continuous task execution. To alleviate this issue, researchers have proposed HATVs [1]–[11], which combine the long-endurance advantage of ground vehicles with the mobility of aerial platforms. Most of these designs are based on quadrotors, leveraging their compact size and vertical takeoff and landing capability for seamless locomotion mode switching.

Despite these advantages, quadrotor-based HATVs suffer from inherent under-actuation: attitude and position control cannot be decoupled. As a result, the vehicle must tilt

This work was supported by the Research Grants Council of Hong Kong SAR under Grants 14217922, 14209623 and 14209424.

¹All authors are with the Department of Mechanical and Automation Engineering, The Chinese University of Hong Kong, Shatin, Hong Kong. (Emails: {rywang, xcliu, zzwu, zxguo, wd.ding}@link.cuhk.edu.hk, bchen@cuhk.edu.hk).

²Ruoyu Wang is also with the Faculty of Engineering, The University of Hong Kong, Pokfulam, Hong Kong.

³Xuchen Liu is also with the Peng Cheng Laboratory, Shenzhen, Guangdong, China.



Fig. 1. Tilt-Ropter: a novel hybrid aerial-terrestrial vehicle.

its body to generate forward thrust, which produces undesired vertical forces during ground locomotion and reduces efficiency. To overcome such limitations of conventional quadrotor-based aerial robots, researchers have explored fully actuated MAVs (FAMAVs), which can generate arbitrary forces and torques in six degrees of freedom. This capability enables independent control of translation and rotation, making FAMAVs a promising basis for HATVs, particularly in scenarios requiring efficient ground locomotion or physical interaction [12]–[14]. Nevertheless, actuation redundancy introduces challenges in control allocation, and the coexistence of multiple locomotion modes further complicates the control problem.

In this work, we present the design of *Tilt-Ropter*, a novel hybrid aerial-terrestrial vehicle that integrates tilt rotors with two passive wheels, as shown in Fig. 1. This configuration enables efficient locomotion both in the air and on the ground, with thrust generated directly along the direction of motion to improve maneuverability. To address the challenges of redundant actuation and multi-modal locomotion, we design a unified wrench-based NMPC framework that incorporates actuator constraints and ground-specific non-holonomic conditions. To further improve robustness during terrestrial locomotion and environmental interaction, an external wrench estimation method tailored to the tilt-rotor system is integrated, allowing the controller to compensate for ground reaction wrenches and external disturbances in real time.

The main contributions of this work are summarized as:

- A novel hybrid aerial-terrestrial vehicle, Tilt-Ropter, featuring tilt rotors and passive wheels, is designed and

implemented.

- A unified dynamic model and nonlinear model predictive controller are developed to achieve optimal performance across both aerial and terrestrial locomotion.
- An external wrench estimation method that accounts for servo dynamics is proposed to accurately estimate interaction forces acting on the robot.

II. RELATED WORKS

A. Hybrid Aerial-Terrestrial Vehicles

These platforms integrate aerial agility with ground mobility, allowing for energy-efficient long-distance traversal and agile obstacle avoidance via flight. Existing designs can be broadly classified by their ground locomotion mechanisms.

1) *Passive Wheel Designs*: Many HATVs adopt passive wheel structures to achieve terrestrial mobility with minimal mechanical complexity. Kalantari *et al.* [1] enclosed a quadrotor in a freely rotating cage, enabling ground motion without additional actuators. However, friction between the cage and ground reduces maneuverability. More recent works [2]–[4] introduced two side-mounted passive wheels, improving flexibility while keeping the additional mass low. Nonetheless, these designs remain underactuated and rely solely on differential thrust for yaw control, limiting precise ground steering.

To further reduce mechanical complexity, some designs employ a single passive wheel mounted on a quadrotor or bi-copter platform [6], [8], [10]. Although this setup minimizes weight, it introduces static instability during terrestrial locomotion and often requires extra energy to maintain balance.

2) *Active Wheel Designs*: Active wheel mechanisms have been explored to enhance ground agility. Sihite *et al.* and Mandralis *et al.* [15], [16] proposed systems with belt-driven wheels and differential steering, enabling omnidirectional motion and smooth transitions. However, the added mechanisms increase the system weight to over 5 kg, significantly compromising flight performance and endurance. Shi *et al.* [17] introduced transformable wheels for flying, rolling, and climbing, with shared actuators to reduce weight, but the use of six actuators and timing belts adds design complexity and weight. A decoupled design was presented by Cao *et al.* [18], which combines a bi-copter and a two-wheeled differential drive. While offering independent control in both modes, its complexity and added mass limit flight agility.

B. Fully-Actuated Micro Air Vehicles

Most HATVs are built upon underactuated quadrotors or bi-copters [1]–[11], where the coupling of attitude and position control limits maneuverability, particularly in yaw and lateral motion. While bi-copters offer improved yaw control via rotor tilting [9], [11], they still face constraints in agile multi-directional maneuvers.

While most HATVs remain underactuated, recent progress in the MAV field has produced fully actuated designs [19]–[21], introducing actuation schemes beyond conventional quadrotors, with potential benefits for future HATV development. Such platforms can in principle generate arbitrary

forces and torques [13], [14], enabling precise 6-DoF control and improved interaction with the environment. However, realizing this capability in practice requires a dedicated control allocation formulation to map the desired wrench to actuator commands and to coordinate multiple actuators, which becomes particularly critical in hybrid locomotion scenarios.

C. Control for Hybrid Aerial and Terrestrial Vehicles

Controlling HATVs requires handling mode transitions and distinct dynamics in each mode. Model-free approaches, particularly PID controllers, are widely adopted for their simplicity [2], [3], [6], [8]–[10], [22], [23], typically using a cascaded structure for position, attitude, and rate control. However, these methods often oversimplify ground interaction and lack robustness during mode transitions.

Model-based methods offer improved performance by leveraging accurate system dynamics [4], [5], [11], [16]. For example, Zhang *et al.* [4] achieved trajectory tracking at up to 3 m/s, while Lin *et al.* [11] demonstrated stable control on slippery terrain. Despite their advantages, most existing methods are tailored to underactuated platforms, limiting their applicability to more complex, fully actuated systems. In this work, we aim to bridge this gap by presenting a fully-actuated hybrid aerial-terrestrial platform along with a unified model-based control approach.

III. SYSTEM DESIGN

A. Mechanical Design

Tilt Ropter is a tilt-rotor quadcopter integrated with two passive wheels, enabling seamless transitions between aerial and terrestrial locomotion. The quadcopter comprises a central base frame and four articulated tilt arms. Each arm is equipped with a T-Motor F80 Pro brushless DC (BLDC) motor, paired with a Foxeer 5145 Donut toroidal propeller.

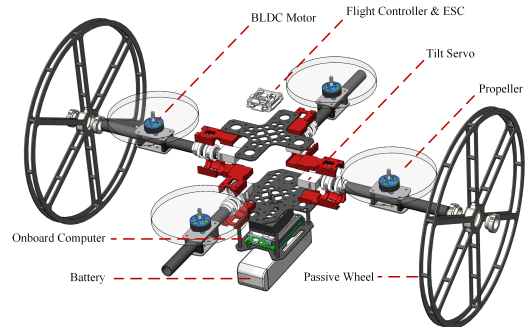


Fig. 2. Exploded view of Tilt-Ropter key components.

The tilt mechanism for each arm is actuated by a GDW RS0708 servo motor, which is mounted within the base frame of the vehicle. Unlike conventional tilt-rotor MAV designs [19], [21], where servo motors are typically positioned at the end of the tilt arms, Tilt Ropter's configuration concentrates the mass closer to the vehicle's center. This centralized layout minimizes the moment of inertia, enhancing the agility and responsiveness. The detailed design of the robot is shown in Fig. 2.

While the centralized design benefits the overall performance of the vehicle, it also presents a challenge: tilting torque must be transmitted to the motor through the arm rather than being applied directly. This indirect transmission path can introduce additional vibrations into the system when structural clearance is present, potentially degrading control performance [24]. To address this issue, three ceramic bearings are utilized to support the tilt mechanism, thereby increasing structural rigidity and eliminating mechanical backlash. The tilt arm is constructed from a 16 mm diameter carbon fiber tube and is connected to the servo motor via an internal coupling. Bushings are used to interface the arm with ceramic bearings, ensuring smooth rotation. The entire assembly, including the tilt arm, bearings, and servo motor, is integrated into two structural shells, which secure their relative positions and further eliminate mechanical clearance. This modular design, as shown in Fig. 3, also allows for easy assembly and disassembly, facilitating maintenance and repairs in real world applications.

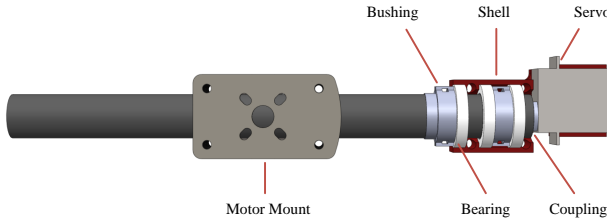


Fig. 3. Illustration of the design of the tilt arm.

Distinct from conventional quadrotor-based HATVs, which usually require additional supporting structures to mount wheels, Tilt-Ropter adopts an innovative design in which two opposing tilt arms serve directly as axles for the passive wheels. Since only the wheels themselves are added, this configuration greatly reduces both structural weight and overall complexity. Passive wheels were deliberately chosen for their simplicity, lightweight nature, and minimal additional energy consumption during ground locomotion.

B. Hardware System Design

The hardware architecture of the Tilt-Ropter integrates power distribution and signal flow across all onboard components. The battery provides the main power supply, delivering energy directly to the Electronic Speed Controller (ESC) and a dedicated Battery Elimination Circuit (BEC). Most electronic devices, including the ESC and flight controller, operate directly from battery voltage, while the servo motors are supplied by a regulated 6 V output from the BEC to ensure stable and reliable performance.

The flight controller (Holybro Kakute H7 V1.3) serves as the low-level unit, acquiring sensor data in real time and performing control allocation to convert high-level force and torque commands into motor and servo commands. Higher-level computation—including model-based control, state estimation, perception, and motion planning—is carried out on an NVIDIA Jetson Orin NX running Ubuntu 20.04 with ROS.

Table I details the models and weights of the key hardware components employed in the Tilt-Ropter. The fully assembled Tilt-Ropter, equipped with a ACE 5300 mAh 45C battery, weighs only about 1.5 kg, which is comparable to a conventional quadrotor.

TABLE I
MODELS AND WEIGHTS OF KEY HARDWARE COMPONENTS

Component	Model	Weight (g)
Battery	ACE 5300 mAh 45C	485
Servo motors	GDW RS0708	145
Onboard computer	NVIDIA Jetson Orin NX	150
Brushless motors	T-Motor F80 Pro	146
Propellers	Foxeer 5145 Donut	20
ESC	Holybro Tekko32 60A	14
Flight controller	Holybro Kakute H7 V1.3	8

IV. MODELING

A. Frame Definition

Throughout this work, we introduce eight coordinate frames, as shown in Fig. 4. The fixed East-North-Up (ENU) inertial frame \mathcal{F}_I . The body frame, \mathcal{F}_B , is attached to the center of mass (CoM) of the robot. Four rotor frames, $\mathcal{F}_{R,i}$ ($i = 1, 2, 3, 4$) are each defined with their origins at the intersection of the propeller's axis of rotation and the central axis of the respective arm. Rotor 1 and rotor 2 rotate in the counterclockwise direction, whereas rotor 3 and rotor 4 rotate in the clockwise direction. The x -axis of each $\mathcal{F}_{R,i}$ aligns with the central axis of its arm and points outward from the CoM. Additionally, two wheel frames, $\mathcal{F}_{W,i}$ ($i = 1, 2$), are introduced, where each frame's origin is located at the geometric center of the wheel. The x -axis of each $\mathcal{F}_{W,i}$ is aligned with the y -axis of \mathcal{F}_B .

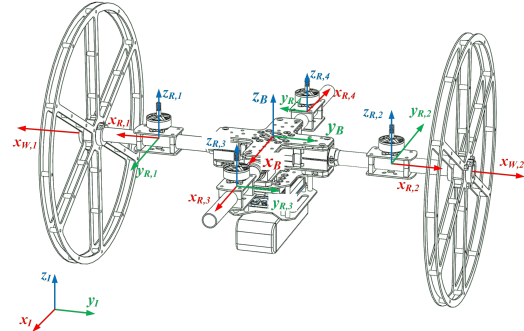


Fig. 4. Definition of coordinate frames.

B. Rigid Body Dynamics

Assuming that Tilt-Ropter can be modeled as a rigid body with mass m and inertia \mathbf{J} , which is driven by the total force \mathbf{F} and torque \mathbf{M} of actuators acting on the CoM, and the gravity $\mathbf{g} = [0, 0, -9.81] \text{ m} \cdot \text{s}^{-2}$.

$$\dot{\mathbf{p}} = \mathbf{v} \quad (1a)$$

$$\dot{\mathbf{q}} = \frac{1}{2} \mathbf{q} \otimes \begin{bmatrix} 0 \\ \boldsymbol{\omega} \end{bmatrix} \quad (1b)$$

$$\dot{\mathbf{v}} = \mathbf{m}^{-1} \mathbf{q} \odot (\mathbf{F} + \mathbf{F}_e) + \mathbf{g} \quad (1c)$$

$$\dot{\boldsymbol{\omega}} = \mathbf{J}^{-1} (\mathbf{M} + \mathbf{M}_e - \boldsymbol{\omega} \times (\mathbf{J} \boldsymbol{\omega})) \quad (1d)$$

where \otimes and \odot denote the multiplication between quaternions and multiplication between a quaternion and a vector, respectively. $\mathbf{p} \in \mathbb{R}^3$ and $\mathbf{v} \in \mathbb{R}^3$ are the position and velocity of CoM in \mathcal{F}_I . $\mathbf{q} \in \mathbb{R}^4$ and $\boldsymbol{\omega} \in \mathbb{R}^3$ are the quaternion and angular velocity of the body frame \mathcal{F}_B . $\mathbf{F}_e \in \mathbb{R}^3$ and $\mathbf{M}_e \in \mathbb{R}^3$ are the external force and torque in the body frame \mathcal{F}_B when the robot is in contact with the environment. It should be noted that \mathbf{F}_e and \mathbf{M}_e , obtained from the external wrench estimation module, cover not only ground contact interactions but also a wide range of robot–environment interactions (e.g., contact wrenches during manipulation) and external disturbances (e.g., wind), thereby extending the applicability of the model to diverse scenarios.

C. Control Allocation

Tilt-Ropter is a fully actuated aerial vehicle, capable of producing arbitrary six-dimensional wrenches. However, unlike a conventional quadrotor with a fixed allocation matrix, the mapping from wrench to actuator commands in this platform is nontrivial. Each tilt-rotor generates a wrench \mathbf{W}_i , which results from the combined effects of rotor thrust T_i and servo tilt angle α_i . A dedicated control allocation formulation is therefore required to consistently convert wrench commands into feasible actuator inputs, while also revealing implicit constraints such as the limited servo rate that will be incorporated later in the NMPC formulation.

Here we neglect the angular acceleration and gyroscopic effects of the rotors, and the thrust T_i is proportional to the square of the rotor speed Ω_i . The relationship between the wrench command and actuator inputs is given by:

$$\begin{aligned} \mathbf{W} &= \begin{bmatrix} \mathbf{F} \\ \mathbf{M} \end{bmatrix} = \mathbf{AT}, \\ \mathbf{T} &= \begin{bmatrix} T_{1,l} \\ T_{1,v} \\ \vdots \\ T_{4,l} \\ T_{4,v} \end{bmatrix} = c_t \begin{bmatrix} \sin(\alpha_1)\Omega_1^2 \\ \cos(\alpha_1)\Omega_1^2 \\ \vdots \\ \sin(\alpha_4)\Omega_4^2 \\ \cos(\alpha_4)\Omega_4^2 \end{bmatrix} \end{aligned} \quad (2)$$

where \mathbf{A} is the control allocation matrix, \mathbf{T} is an intermediate thrust vector defined in the body frame \mathcal{F}_B . The vector \mathbf{T} decomposes the rotor thrust into the lateral and vertical components, with thrust coefficient represented by c_t . By introducing \mathbf{T} , the effect of servo angle α on rotor thrust T is incorporated directly into the thrust vector, thereby simplifying the control allocation matrix. This formulation makes the control allocation matrix \mathbf{A} a static matrix that depends only on the fixed geometry of the robot and is independent of the dynamic tilt angles. So we can calculate the intermediate thrust vector \mathbf{T} using Moore–Penrose pseudoinverse:

$$\mathbf{T} = \mathbf{A}^\dagger \mathbf{W} \quad (3)$$

The thrust T_i of the i -th rotor can be calculated as:

$$T_i = \sqrt{T_{i,l}^2 + T_{i,v}^2} \quad (4)$$

Then the rotor angular speed Ω_i and servo angle α_i can be obtained by:

$$\begin{aligned} \Omega_i &= \sqrt{\frac{T_i}{c_t}}, \\ \alpha_i &= \text{atan2}(T_{i,v}, T_{i,l}) \end{aligned} \quad (5)$$

Given the relationship between the servo angle α and the thrust vector \mathbf{T} , we can deduce the corresponding relationship between the servo angle speed $\dot{\alpha}$ and the wrench change rate $\dot{\mathbf{W}}$:

$$\begin{aligned} \dot{\alpha}_i &= \frac{\dot{T}_{i,l}T_{i,v} - T_{i,l}\dot{T}_{i,v}}{T_{i,v}^2 + T_{i,l}^2}, \\ \dot{T}_{i,l} &= (\mathbf{A}^\dagger \dot{\mathbf{W}})_{2i-1}, \\ \dot{T}_{i,v} &= (\mathbf{A}^\dagger \dot{\mathbf{W}})_{2i}. \end{aligned} \quad (6)$$

The relationship between the servo angle speed and wrench change rate shown in Eq. (6) reveals a critical insight into the system dynamics. When the wrench changes rapidly, it directly impacts the required servo angle speeds. Since servos typically have slower dynamics compared to the BLDC motors, excessively rapid wrench changes can cause the servos to lag behind commanded angles. This lag creates a mismatch between the commanded and actual thrust vectors, potentially leading to oscillations and instability in the system. Therefore, the wrench change rate must be carefully constrained in controller to remain within the physical limitations of the servo dynamics, ensuring smooth and stable performance of the Tilt-Ropter system.

V. CONTROL

In this section, we present the control design for the Tilt-Ropter. The overall architecture is shown in Fig. 5. The motion planner generates reference trajectories, which are tracked by a nonlinear model predictive controller. Based on the control allocation formulation in Sec. IV-C, the NMPC is formulated with wrench command \mathbf{W} as its output, instead of directly commanding rotor speeds and servo angles. Although actuator-level NMPC could exploit the full actuation property of the platform, its higher input dimensionality and computation cost hinder real-time feasibility. In contrast, the wrench-based NMPC retains efficiency while incorporating actuator constraints, and generally provides superior power efficiency and tracking accuracy except under highly aggressive maneuvers [25].

The optimal wrench command is then mapped to actuator commands through control allocation and executed by the motors and servos. State estimation is performed by an Extended Kalman Filter (EKF), which fuses inertial measurements with motion capture data to provide accurate pose and attitude. In addition, the external wrench acting on the robot is estimated to compensate for the external force and torque. Overall, the control architecture ensures accurate trajectory tracking while maintaining stability and robustness under environmental interactions.

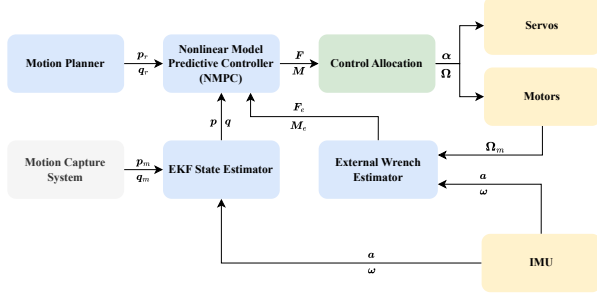


Fig. 5. Control architecture of Tilt-Ropter. p_m and q_m are the measured position and quaternion of the robot from motion capture system. Ω_m is the measured rotor speeds from ESC.

A. Nonlinear Model Predictive Control

The control problem is formulated as a finite-time optimal control problem (OCP), where the objective is to minimize the tracking error of the robot state and input to the reference trajectory while satisfying the system dynamics and constraints. Additionally, NMPC enables smooth interaction between the robot and the ground by incorporating contact wrenches into the dynamic model and formulating ground-specific constraints within the control problem. This approach provides a unified control architecture for both aerial and terrestrial locomotion, facilitating seamless transitions between modes.

1) *States and Inputs*: Firstly, we choose the system state x and control inputs u as:

$$x = [F^\top \ M^\top \ p^\top \ v^\top \ q^\top \ \omega^\top]^\top \in \mathbb{R}^{19}, \quad (7a)$$

$$u = [\dot{F}^\top \ \dot{M}^\top]^\top \in \mathbb{R}^6. \quad (7b)$$

Noted that the NMPC does not directly optimize the wrench command W , but rather its derivative \dot{W} as the control input. This choice implicitly incorporates the actuator dynamics, particularly the slower servo responses, into the optimization process.

2) *Problem Formulation*: Accordingly, the NMPC optimization problem is formulated as:

$$\begin{aligned} u_{\text{NMPC}} = \arg \min_u & \sum_{k=0}^{N-1} (\tilde{x}_k^\top Q \tilde{x}_k + u_k^\top R u_k) \\ & + \tilde{x}_N^\top Q_N \tilde{x}_N \end{aligned} \quad (8a)$$

subject to $x_0 = x_{\text{est}}$,

$$\begin{aligned} x_{k+1} &= f(x_k, u_k), \\ u_k &\in [-u_{\text{max}}, u_{\text{max}}], \\ W_k &\in [W_{\text{min}}, W_{\text{max}}], \\ \delta \cdot v_{B,y} &= 0, \\ \delta \cdot \omega_x &= 0, \\ \delta \cdot (p_z - r) &= 0. \end{aligned} \quad (8b)$$

where N is the length of prediction horizon. Q and Q_N are the stage and terminal state cost matrices, respectively. R is the cost matrix for the control input. x_{est} is the current estimated state of the robot. The system dynamics

are described by f , the discrete-time formulation of the continuous dynamics given in (1a)-(1d). The input bounds u_{max} restrict the rate of change of the commanded wrench. These bounds also implicitly enforce the servo rate limitation derived in Sec. IV-C, ensuring that the generated actuator commands remain dynamically feasible. W_{min} and W_{max} are the constraints on the wrench command, ensuring the robot safety and stability.

The non-holonomic constraints on the ground are formulated using a indicator function δ , defined as:

$$\delta = \begin{cases} 1, & \text{if } p_{r,z} = r \text{ and } p_z = r \\ 0, & \text{otherwise} \end{cases} \quad (9)$$

where $p_{r,z}$ is the reference height from motion planner, p_z is the current height of the robot, and r is the radius of the wheel. The indicator function δ is used to activate or deactivate the non-holonomic constraints based on the robot's state. Only when the robot is on the ground ($p_z = r$) and the reference trajectory is a ground trajectory ($p_{r,z} = r$), the non-holonomic constraints are activated. In Eq. (8b), the last three constraints impose the non-holonomic conditions when the robot is on the ground. Specifically, the first constraint ensures that the robot does not move in the y -direction. Note that the velocity $v_{B,y}$ is the y -component of the velocity in the body frame \mathcal{F}_B . The second constraint prevents rotation about the x -axis. The third constraint ensures that the robot maintains contact with the ground by keeping the height equal to the wheel radius. These constraints are crucial for maintaining stability and preventing undesired motion during ground locomotion.

The state tracking error \tilde{x} at time step k is defined as:

$$\tilde{x}_k = \begin{bmatrix} F_k \\ M_k \\ p_k - p_{r,k} \\ v_k - v_{r,k} \\ \tilde{x}_{q,k} \\ \omega_k - \omega_{r,k} \end{bmatrix} \quad (10)$$

where $p_{r,k}$, $v_{r,k}$, $q_{r,k}$, and $\omega_{r,k}$ are the reference position, velocity, quaternion, and angular velocity obtained from the trajectory planner. Since unit quaternions lie on a nonlinear manifold, orientation error is defined as $\tilde{x}_{q,k} = q_k \otimes q_{r,k}^{-1}$, representing the minimal rotation that aligns the current orientation with the reference.

VI. EXTERNAL WRENCH ESTIMATION

The external wrench estimation is essential for the control of Tilt-Ropter, especially when the robot is in contact with the ground. The implementation of the external wrench estimation follows the method introduced in [26]. This approach integrates the advantages of momentum-based and acceleration-based approaches, requiring only measurements of the robot's acceleration and angular velocity. It eliminates the need for a translational velocity sensor, such as optical flow or visual inertial odometry (VIO), and avoids the

numerical differentiation of angular velocity. The external wrench estimation can be expressed as:

$$\begin{aligned}\hat{\mathbf{F}}_e &= \mathbf{K}_f \int (\mathbf{m}\mathbf{a} - \mathbf{F} - \hat{\mathbf{F}}_e) dt, \\ \hat{\mathbf{M}}_e &= \mathbf{K}_m \left(\mathbf{J}\boldsymbol{\omega} - \int (\mathbf{M} + (\mathbf{J}\boldsymbol{\omega}) \times \boldsymbol{\omega} + \hat{\mathbf{M}}_e) dt \right).\end{aligned}\quad (11)$$

where $\mathbf{a} = \mathbf{q}^{-1} \odot (\dot{\mathbf{v}} + \mathbf{g})$ is the measured acceleration of the robot in the body frame. $\hat{\mathbf{F}}_e$ and $\hat{\mathbf{M}}_e$ are the estimated external force and torque acting on the robot, respectively. \mathbf{K}_f and \mathbf{K}_m are the estimation gains. By differentiating Eq. (11), the external wrench estimation can be reformulated as a first-order low-pass filter:

$$\begin{aligned}\dot{\hat{\mathbf{F}}}_e &= \mathbf{K}_f (\mathbf{F} - \hat{\mathbf{F}}_e), \\ \dot{\hat{\mathbf{M}}}_e &= \mathbf{K}_m (\mathbf{M} - \hat{\mathbf{M}}_e).\end{aligned}\quad (12)$$

This reformulation highlights the filtering effect of the estimation process, effectively reducing noise in the raw acceleration and angular velocity measurements from IMU, thereby improving the robustness of the external wrench estimation.

To compute the external wrench applied to the vehicle, it is necessary to determine the total force \mathbf{F} and torque \mathbf{M} generated by the actuators. Only relying on the commanded wrench from the NMPC is not appropriate, as it does not account for the dynamics of the actuators. Instead, a more accurate estimation of the applied wrench can be obtained by computing the resultant force and torque based on the measured rotor speeds and the estimated servo angles. It is important to note that the estimated servo angles are used in place of the actual angles, as typical hobby-grade servo motors lack integrated angle feedback functions. We consider the servo dynamics by incorporating a first-order system model of the servo. The servo dynamics can be expressed as:

$$\dot{\alpha} = \frac{1}{\tau}(\alpha - \alpha_{act}) \quad (13)$$

where $\dot{\alpha}$ denotes the servo angular speed, α is the commanded servo angle provided by the control allocation, α_{act} is the actual servo angle, and τ represents the time constant of the servo. The time constant τ can be identified through system identification techniques, such as step response analysis based on experimental data, as illustrated in Fig. 6. In this process, the servo motor is subjected to a step input, and the resulting angular response is recorded and fitted to a first-order system model using least squares estimation.

With the servo dynamics characterized as a first-order system and the time constant identified, the actual servo angles can be estimated by simulating the servo response to the commanded inputs. These estimated angles, together with the measured rotor speeds, are then substituted into Eq.(2) to compute the total force \mathbf{F} and torque \mathbf{M} generated by the actuators. Subsequently, the external wrench—comprising the estimated external force $\hat{\mathbf{F}}_e$ and torque $\hat{\mathbf{M}}_e$ —can be obtained by substituting the computed \mathbf{F} and \mathbf{M} into Eq. (11).

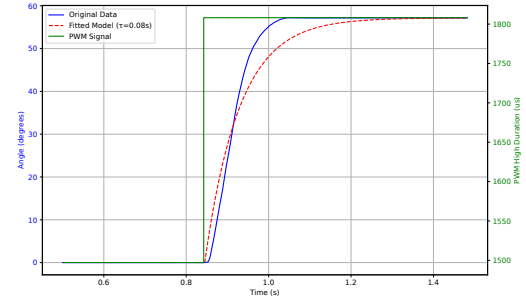


Fig. 6. System identification of the servo with attached motor and propeller. The green line represents the PWM input signal to the servo, the blue line shows the original angle data collected by the rotary encoder, and the red line depicts the fitted response based on the identified first-order model.

This approach enhances the accuracy of the external wrench estimation by explicitly considering actuator dynamics and compensating for the absence of direct servo angle measurements.

VII. EXPERIMENTS AND RESULTS

A. Simulation

To validate the proposed robot configuration and control algorithms, we developed a comprehensive simulation platform for Tilt-Ropter using the Gazebo simulator. We carefully measured and calculated key physical parameters such as mass, CoM, and inertia, ensuring a minimal gap between the simulation and real-world performance. Different from the traditional quadrotor simulation, our simulation incorporates both servo dynamics and the motion of passive wheels. This approach allows us to accurately simulate the tilt-rotor mechanisms and the generation of vector thrust. Additionally, the interaction between the wheels and the ground, including contact forces, is managed by the Open Dynamics Engine (ODE) within Gazebo, providing a realistic representation of on-ground dynamics.

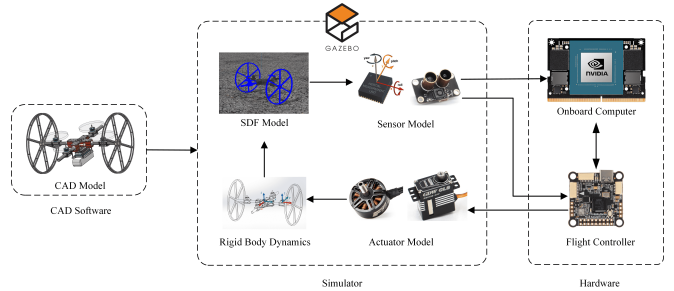


Fig. 7. The structure of hardware-in-the-loop simulation.

Besides the common software-in-the-loop (SITL) simulation, we also developed a hardware-in-the-loop (HITL) simulation to test the algorithms with hardware on the real robot. The structure of HITL simulation is shown in Fig. 7. In our HITL simulation, the real robot is integrated with the simulation environment via the ROS framework. The Gazebo simulator generates virtual sensor data, which is utilized by the state estimation module in the physical onboard computer. Simultaneously, this onboard computer processes

high-level control commands using NMPC algorithms. The control commands are then forwarded to the physical low-level flight controller, which generates actuator commands for the simulated actuators. The state of the simulated robot is dynamically updated based on these commands, guided by the rigid body dynamics model implemented within the simulation. This integration ensures a continuous and accurate exchange of data and control between the real and simulated components, significantly enhancing both the fidelity and effectiveness of the simulation. A demonstration of the simulation results, including air-ground transitions and trajectory tracking, is provided in the supplementary video.

B. Real-World Experiments

We conducted a series of real-world experiments to validate the performance of the Tilt-Ropter. The robot was tested in various scenarios, including aerial flights, ground locomotion, and mode transitions. The results demonstrated the effectiveness of the proposed model-based control algorithms and the versatility of the Tilt-Ropter design. The parameters for the NMPC in these experiments are shown in Table II.

TABLE II
NMPC PARAMETERS FOR REAL-WORLD EXPERIMENTS

Parameter	Value
$\dot{\mathbf{F}}_{max}$	(2, 2, 2) $N \cdot s^{-1}$
$\dot{\mathbf{M}}_{max}$	(2, 2, 2) $N \cdot m \cdot s^{-1}$
\mathbf{F}_{min}	(-0.2, -0.2, 0.0) N
\mathbf{F}_{max}	(0.2, 0.2, 20) N
\mathbf{M}_{min}	(-20, -20, -20) N · m
\mathbf{M}_{max}	(20, 20, 20) N · m
ω_{max}	(2.0, 2.0, 1.5) $rad \cdot s^{-1}$
N	20
Δt	0.1 s

1) *Aerial Flight*: To validate the aerial flight performance of the Tilt-Ropter, a trajectory tracking experiment was conducted. The robot was commanded to follow the trajectory as shown in Fig. 8(a).

The trajectory is a figure-eight shape, which includes both horizontal and vertical movements. The maximum velocity and acceleration of the robot are set to 1.5 m/s and 1.5 m/s^2 respectively. The robot successfully tracked the trajectory with root-mean-square error (RMSE) of 0.052 m, demonstrating the effectiveness of the NMPC-based control algorithms.

2) *Ground Locomotion*: Similar to the aerial flight experiment, we conducted a ground locomotion experiment to evaluate the performance of the Tilt-Ropter in terrestrial mode. The only difference of the trajectory is that the robot is commanded to move on the ground. The robot successfully tracked the trajectory with RMSE of 0.145 m, as shown in Fig. 8(b), demonstrating the effectiveness of the proposed control algorithms in ground locomotion scenarios.

3) *Air-Ground Mode Transition*: To evaluate the air-ground mode transition performance of the Tilt-Ropter, we conducted a trajectory tracking experiment encompassing both aerial flight and ground locomotion phases. The robot starts

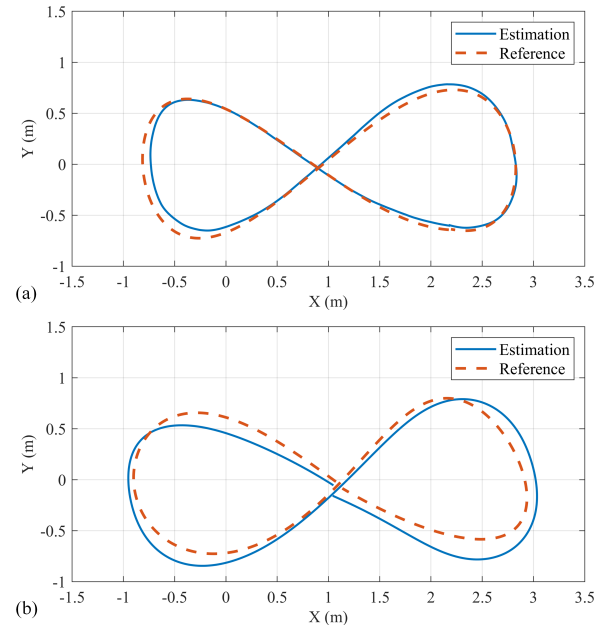


Fig. 8. Trajectories of the Tilt-Ropter in aerial and ground modes. (a) Trajectory of Tilt-Ropter in aerial flight. (b) Trajectory of Tilt-Ropter in ground locomotion.

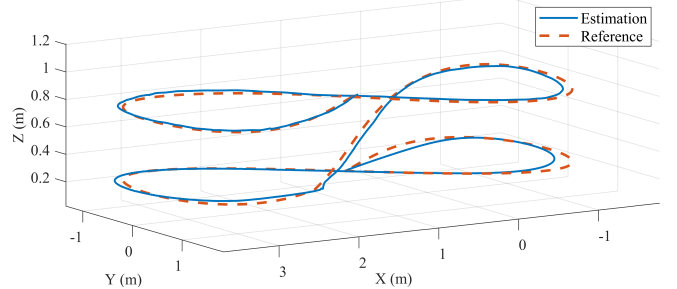


Fig. 9. Hybrid trajectory of Tilt-Ropter showcasing seamless air-ground mode transitions.

from an arbitrary position in the air, follows a figure-eight trajectory with air locomotion mode, then transitions smoothly to the ground, continuing to track a similar figure-eight trajectory on the ground. The trajectory is shown in Fig. 9. The robot successfully completed the trajectory and performed a smooth mode transition between aerial flight and ground locomotion with RMSE of 0.125 m, demonstrating the versatility of the NMPC controller and robustness of the Tilt-Ropter design.

4) *Energy Efficiency*: To analyze the energy efficiency of the Tilt-Ropter design, we compared the power consumption of the robot during aerial flight and ground locomotion scenarios. The robot is given a hybrid trajectory that includes both aerial and ground phases. The power consumption is calculated by multiplying the voltage and current of the battery measured during the experiments. The voltage of the battery is measured by the Analog-to-Digital Converter (ADC) inside the flight controller. And the current is measured by the current sensor within the ESC. The results are shown in Fig. 10. We calculated the average power consumption during the aerial flight and ground locomotion

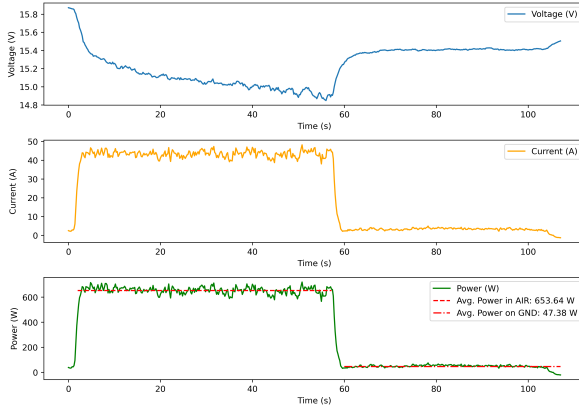


Fig. 10. Comparison of power consumption between aerial flight and ground locomotion.

phases, which are 653.64 W and 47.38 W, respectively. The results indicate that the power consumption of the robot in ground locomotion is only 7.2% of that in aerial flight. This significant reduction in power consumption during ground locomotion highlights the energy efficiency of the Tilt-Ropter design, which makes it an ideal platform for long-endurance missions by leveraging its multi-modal capabilities.

VIII. CONCLUSION

In this work, we present the design, modeling, and control of a novel hybrid aerial-terrestrial vehicle, Tilt-Ropter. By integrating tilt rotors with passive wheels, the platform achieves energy-efficient ground locomotion while preserving aerial agility. A control allocation formulation was introduced to characterize the mapping between actuator inputs and the desired wrench, which in turn enabled a unified NMPC framework for trajectory tracking and smooth transitions across aerial and terrestrial locomotion modes. Furthermore, an external wrench estimation method enhanced robustness during ground contact and environmental interaction. The proposed hybrid aerial-terrestrial system was validated through hardware-in-the-loop simulations and real-world experiments, demonstrating reliable multi-modal locomotion, smooth mode transition, and promising energy efficiency.

REFERENCES

- [1] A. Kalantari and M. Spenko, “Modeling and performance assessment of the hytaq, a hybrid terrestrial/aerial quadrotor,” *IEEE Transactions on Robotics*, vol. 30, no. 5, pp. 1278–1285, 2014.
- [2] R. Zhang, Y. Wu, L. Zhang, C. Xu, and F. Gao, “Autonomous and adaptive navigation for terrestrial-aerial bimodal vehicles,” *IEEE Robotics and Automation Letters*, vol. 7, no. 2, pp. 3008–3015, 2022.
- [3] D. D. Fan, R. Thakker, T. Bartlett, M. B. Miled, L. Kim, E. Theodorou, and A.-a. Agha-mohammadi, “Autonomous hybrid ground/aerial mobility in unknown environments,” in *2019 IEEE/RSJ International Conference on Intelligent Robots and Systems (IROS)*. IEEE, 2019, pp. 3070–3077.
- [4] R. Zhang, J. Lin, Y. Wu, Y. Gao, C. Wang, C. Xu, Y. Cao, and F. Gao, “Model-based planning and control for terrestrial-aerial bimodal vehicles with passive wheels,” in *2023 IEEE/RSJ International Conference on Intelligent Robots and Systems (IROS)*. IEEE, 2023, pp. 1070–1077.
- [5] T. Wu, Y. Zhu, L. Zhang, J. Yang, and Y. Ding, “Unified terrestrial/aerial motion planning for hytaqs via nmpc,” *IEEE Robotics and Automation Letters*, vol. 8, no. 2, pp. 1085–1092, 2023.
- [6] N. Pan, J. Jiang, R. Zhang, C. Xu, and F. Gao, “Skywalker: A compact and agile air-ground omnidirectional vehicle,” *IEEE Robotics and Automation Letters*, vol. 8, no. 5, pp. 2534–2541, 2023.
- [7] M. Cao, J. Zhao, X. Xu, and L. Xie, “Aircrab: A hybrid aerial-ground manipulator with an active wheel,” *arXiv preprint arXiv:2403.15805*, 2024.
- [8] S. Yu, B. Pu, K. Dong, S. Bai, and P. Chirarattananon, “A hybrid quadrotor with a passively reconfigurable wheeled leg capable of robust terrestrial maneuvers,” *IEEE Robotics and Automation Letters*, 2025.
- [9] J. Yang, Y. Zhu, L. Zhang, Y. Dong, and Y. Ding, “Sytab: A class of smooth-transition hybrid terrestrial/aerial bicopters,” *IEEE Robotics and Automation Letters*, vol. 7, no. 4, pp. 9199–9206, 2022.
- [10] Y. Qin, Y. Li, X. Wei, and F. Zhang, “Hybrid aerial-ground locomotion with a single passive wheel,” in *2020 IEEE/RSJ International Conference on Intelligent Robots and Systems (IROS)*. IEEE, 2020, pp. 1371–1376.
- [11] J. Lin, R. Zhang, N. Pan, C. Xu, and F. Gao, “Skater: A novel bi-modal bi-copter robot for adaptive locomotion in air and diverse terrain,” *IEEE Robotics and Automation Letters*, 2024.
- [12] M. Hamandi, F. Usai, Q. Sablé, N. Staub, M. Tognon, and A. Franchi, “Design of multirotor aerial vehicles: A taxonomy based on input allocation,” *The International Journal of Robotics Research*, vol. 40, no. 8-9, pp. 1015–1044, 2021.
- [13] K. Bodie, M. Brunner, M. Pantic, S. Walser, P. Pfändler, U. Angst, R. Siegwart, and J. Nieto, “Active interaction force control for contact-based inspection with a fully actuated aerial vehicle,” *IEEE Transactions on Robotics*, vol. 37, no. 3, pp. 709–722, 2020.
- [14] K. Bodie, Z. Taylor, M. Kamel, and R. Siegwart, “Towards efficient full pose omnidirectionality with overactuated mavs,” in *Proceedings of the 2018 International Symposium on Experimental Robotics*. Springer, 2020, pp. 85–95.
- [15] E. Sihite, A. Kalantari, R. Nemovi, A. Ramezani, and M. Gharib, “Multi-modal mobility morphobot (m4) with appendage repurposing for locomotion plasticity enhancement,” *Nature communications*, vol. 14, no. 1, p. 3323, 2023.
- [16] I. Mandralis, R. Nemovi, A. Ramezani, R. M. Murray, and M. Gharib, “Atmo: An aerially transforming morphobot for dynamic ground-aerial transition,” *arXiv preprint arXiv:2503.00609*, 2025.
- [17] K. Shi, Z. Jiang, L. Ma, L. Qi, and M. Jin, “Mtabot: An efficient morphable terrestrial-aerial robot with two transformable wheels,” *IEEE Robotics and Automation Letters*, vol. 9, no. 2, pp. 1875–1882, 2024.
- [18] M. Cao, X. Xu, S. Yuan, K. Cao, K. Liu, and L. Xie, “Doublebee: A hybrid aerial-ground robot with two active wheels,” in *2023 IEEE/RSJ International Conference on Intelligent Robots and Systems (IROS)*. IEEE, 2023, pp. 6962–6969.
- [19] M. Ryll, H. H. Bülthoff, and P. R. Giordano, “A novel overactuated quadrotor unmanned aerial vehicle: Modeling, control, and experimental validation,” *IEEE Transactions on Control Systems Technology*, vol. 23, no. 2, pp. 540–556, 2014.
- [20] M. Kamel, S. Verling, O. Elkhatib, C. Sprecher, P. Wulkop, Z. Taylor, R. Siegwart, and I. Gilitschenski, “Voliro: An omnidirectional hexacopter with tilttable rotors,” *arXiv preprint arXiv:1801.04581*, 2018.
- [21] J. Li, J. Sugihara, and M. Zhao, “Servo integrated nonlinear model predictive control for overactuated tilttable-quadrotors,” *IEEE Robotics and Automation Letters*, 2024.
- [22] Q. Guo, Z. Guo, Y. Shi, Z. Zhou, and D. Ma, “A multimodal agile land-air aircraft (ala) that can fly, roll, and stand,” *Journal of Field Robotics*, 2024.
- [23] Y. Dong, Y. Zhu, L. Zhang, and Y. Ding, “Tactv: A class of hybrid terrestrial/aerial coaxial tilt-rotor vehicles,” *arXiv preprint arXiv:2411.12359*, 2024.
- [24] X. Liu, M. Dou, D. Huang, S. Gao, R. Yan, B. Wang, J. Cui, Q. Ren, L. Dou, Z. Gao, et al., “Tj-flyingfish: Design and implementation of an aerial-aquatic quadrotor with tiltable propulsion units,” in *2023 IEEE International Conference on Robotics and Automation (ICRA)*. IEEE, 2023, pp. 7324–7330.
- [25] M. Brunner, W. Zhang, A. Roumieu, M. Tognon, and R. Siegwart, “Mpc with learned residual dynamics with application on omnidirectional mavs,” *arXiv preprint arXiv:2207.01451*, 2022.
- [26] T. Tomic, C. Ott, and S. Haddadin, “External wrench estimation, collision detection, and reflex reaction for flying robots,” *IEEE Transactions on Robotics*, vol. 33, no. 6, pp. 1467–1482, 2017.